

## Contents lists available at ScienceDirect

# Wear

journal homepage: www.elsevier.com/locate/wear





# Current-carrying tribological properties of an elastic roll ring under different currents

Tianhua Chen<sup>a</sup>, Chenfei Song<sup>a,\*</sup>, Zili Liu<sup>b</sup>, Li Wang<sup>b</sup>, Xinbin Hou<sup>b</sup>, Huanhuan Lu<sup>a</sup>, Yongzhen Zhang<sup>a</sup>

a National United Engineering Laboratory for Advanced Bearing Tribology, Henan University of Science and Technology, Luoyang, 471023, Henan Province, PR China

#### ARTICLE INFO

#### Keywords: Current Wear Roll ring

Hardness

# ABSTRACT

A novel rotating conductive joint that comprises an inner raceway, outer raceway, and a roll ring is proposed in this study. The tribological and conductive properties of the rolling rings were studied under current conditions of 0–20 A. The current density of the rolling contact reached 419 A/mm<sup>2</sup> when transmitted at 20 A. However, a high current could result in a high-friction coefficient and severe wear. The results of optical microscopy and electron back-scattered diffraction showed that the grain boundary was partially annihilated, and the stress decreased in the wear area under 10 and 20 A. On the wear surface, the current-carrying friction caused the hardening, and the electroplasticity caused softening. The surface hardness of the wear area was the result of competition between hardening and softening, which reached its highest value at 5 A.

#### 1. Introduction

Rotating electrical connectors are used in many electromechanical systems that include man-made space stations, satellites, radars, and wind turbines [1]. Conventional electrical transmission devices primarily utilize the sliding electrical contact between the brushes and conductive rings to transmit power/signals [2]. The performance of electric transmission is significantly affected by the combined effects of the current and sliding movement. In particular, under high current conditions, abnormal wear, are ablation, and oxidation are inevitable disadvantages of sliding electrical contact pairs.

Mei et al. [3] reported that the wear volume of a slider increased with the electric current; in addition, arc melting and thermally enhanced wear were reported as the dominant mechanisms causing severe damage to the slider. Ding et al. [4] observed that the friction coefficient decreased significantly with the electric current and suggested that the electric current induced a lubrication effect owing to the formation of oxidation layers at the interface. Ren et al. [5] studied the effects of current on the wear and fretting corrosion of gold-plated copper pairs, and the results indicated that the melting of the metal and breakdown of oxide films under higher currents were the main wear mechanisms. Feng et al. [6] observed that the wear loss in the presence of an electric current was greater than that without a current, which resulted from

roughening and weakening of a counter surface induced by current heating. Fadin et al. [7] reported that the intensity of surface destruction increases with the current density. The coupling effect of friction and current results in the build-up of heat at the contact interface, which can result in the weakening of material performance, oxidation, and even arcing. Therefore, the transmission capacity of sliding electrical contact pairs is limited.

A gentler frictional motion is introduced into rotating conductive devices to weaken the coupling between friction and conduction. A rolling electrical transmission device has been invented, which contains inner raceways, outer raceways, and flexible rings assembled between raceways [1]. When the two raceways rotate relative to each other, the rings are captured and forced to roll owing to the friction force. Therefore, the contact region between the roll rings and raceways simultaneously withstands friction, and the electric current forms a current-carrying contact [8,9]. However, the interaction between current and rolling friction has rarely been reported. The current transmission characteristics in the roll ring and wear behaviors in the contact area remain unclear.

In this study, the tribological and conductive characteristics of a roll ring were analyzed. The influence of current on rolling wear was analyzed in detail from the perspectives of temperature increase, hardness, grain deformation, and stress. These results may provide useful

E-mail address: cfsong@haust.edu.cn (C. Song).

b Qian Xuesen Laboratory, China Academy of Space Technology, Beijing, 100094, PR China

<sup>\*</sup> Corresponding author.

support for the design and operation of rolling electric transmission devices.

## 2. Experimental details

#### 2.1. Materials and tests

As shown in Fig. 1, the friction pairs comprised an outer raceway, an inner raceway, and a roll ring. The copper–beryllium alloy (GB/T 5231-2001), after aging treatment, was selected for all the components because of its excellent elastic stability, high strength, and good electrical conductivity; they were purchased from Shanghai Kaixin Metal Materials Co., Ltd. Before each test, the contact surfaces of the roll rings (end faces) were ground using silicon carbide waterproof sandpaper in the order of 800, 1000, and 1500 grit and polished with a  $3.5~\mu m$  diamond suspension using an Mp-2B metallographic polishing machine. The raceways were also ground with silicon carbide waterproof sandpaper in the order of 800, 1000, and 1500 grit.

A current-carrying tribometer (VCF-SR40, Lanzhou Huahui Instrument Technology Co., Ltd, China) was used to measure the current-carrying properties of the roll ring. As shown in Fig. 1b, the outer raceway was mounted on the suspension, and the inner raceway was mounted on the central axis. After the value of the elastic force and torque was adjusted to zero, the roll ring was assembled between the two raceways. The diameter of the roll-ring is slightly larger than the radial space between the two raceways, such that a compressed elastic force would be generated. The central axis was driven by a servo motor, the inner raceway was rotated, and the roll ring was pushed to the roll. The electric current was supplied by direct voltage power (DC), which was passed through the inner raceway, roll ring, and outer raceway, and then returned to the DC source (Fig. 1c). Details of the experimental conditions are listed in Table 1.

The calculation of the elastic force, contact resistance, and friction force of the contact points is described in Reference [8]. The total number of rolling cycles was set to 108000 for all the tests to achieve a stable wear state. The tests were performed under ambient atmospheric conditions, at room temperature (20  $\pm$  5  $^{\circ}$ C) and relative humidity (50  $\pm$  2%). The tests for each operating condition were repeated five times.

# 2.2. Analysis

Before and after each test, the mass of the elastic roll ring was weighed using an electronic balance (FA224C, Shanghai China) with an accuracy of 0.1 mg. The wear loss of the roll rings was represented by the mass loss after the tests. The raceway was V-shaped, and the wear area was on the sidewall of the raceway, which was very difficult to observe. In addition, the elastic roll ring was easy to manufacture and replace. Therefore, the elastic roll ring is the primary focus of this paper. A 3D surface profiler (Nano Focus-AG, Germany) was used to measure the surface roughness of the contact area. The hardness was measured using a microhardness tester (HV-1000, China) under a load of 200 gf and a duration of 15 s. Each sample was measured at least five times. According to the ASTM E384-2016 standard, a tetragonal pyramid

Table 1
Details of experimental conditions.

Test conditions	Value/units	
Radius of inner raceway	59 mm	
Radius of outer raceway	124 mm	
Elastic force	20.4 N	
Compression deformation	3 mm	
Current	0 A, 2.5 A, 5 A, 10 A, 20 A	
Rotation speed of inner raceway	600 r/min	

diamond indenter was used to measure microhardness. After the indenter was pressed for 3 s, the load reached its maximum, and the material yielded. The shear strain rate of the hardness test was estimated as  $0.17\ 1/s$  because the shear stress at yield was  $1195\ MPa$  and the shear modulus was  $55652.17\ MPa$  [10]. An infrared thermometer (Smart Sensor AS852B, China) was used to measure contact temperature.

The wear location, specific sample section preparation method and observations direction were described in Fig. 2. The elastic rings were placed on the bottom of the grinding tool and were covered by Bakelite powder. Then, the Bakelite was cured by hot press sintering. After curing, the bottom of the Bakelite resin was flush with the edge of the elastic ring. Then, the resin bottom was ground with abrasive paper along the thinning direction in Fig. 2b, and polished with a microndiamond particle paste. The thinning thickness was calculated according to the wear mark width, so that the exposed interface was below the center of wear mark. The samples were then etched using a mixture of 8 g CuCl $_2$  + 92 mL NH $_3$ ·H $_2$ O. Finally, the subsurface in section direction was exposed to the observer. To analyze the wear mechanism, the worn surfaces were observed using scanning electron microscopy (SEM, JSM-IT100, JEOL, Japan) equipped an energy dispersive spectrometer (EDS, EDAX Octane SDD Series, USA) and optical microscopy (OM, DMi 8C, Leica, Germany). The grain deformation beneath the wear scar was characterized using electron backscattered diffraction (EBSD, EDAX-TSL Oxford Nordly max 3).

## 3. Results and discussion

#### 3.1. Tribological and conductive behaviors

The real-time total friction force at different electric current levels is shown in Fig. 3a. The friction force for all the tests experienced two stages, namely, a short running-in process and a stable stage. This revealed that an increase in the electric current resulted in a significant increase in the friction force. The minimum frictional force that occurred at 2.5 A was about 9.89 N, whereas the friction force increased to 14.31 N when the electric current reached 20 A. A test without an electric current was conducted for comparison, and the value of friction force was found to be relatively small at about 6.8 N.

Contact resistance is another important property of current-carrying devices. The variations in the contact resistance as a function of the rolling revolutions at different currents are shown in Fig. 3b. The contact resistance was characterized by two distinct stages. First, the contact resistance increased rapidly and then decreased after reaching the peak

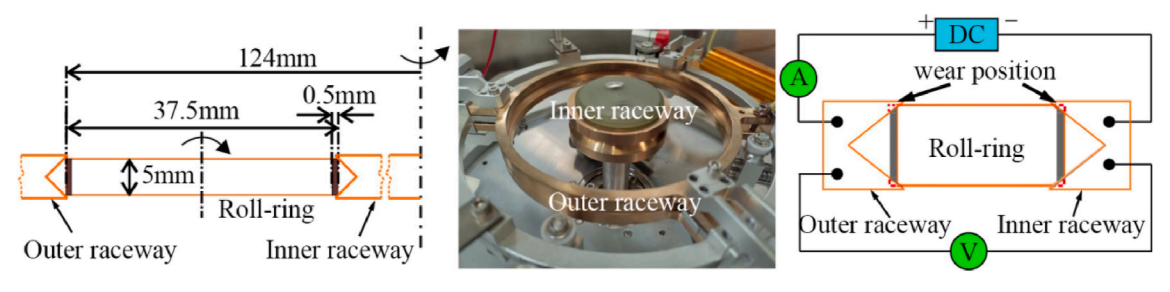


Fig. 1. Introduction of current-carrying friction pairs.

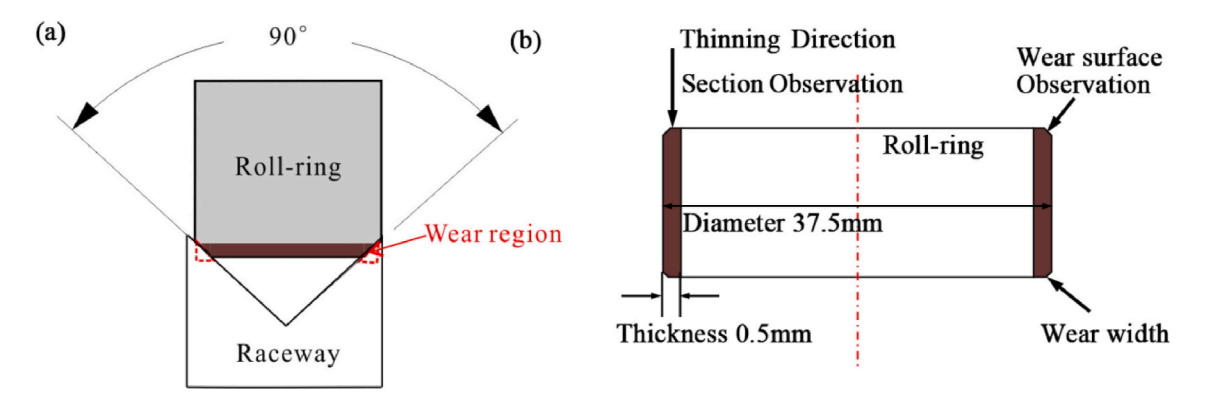


Fig. 2. The sketch of (a) contact region between roll-ring and raceways and (b) observation positions.

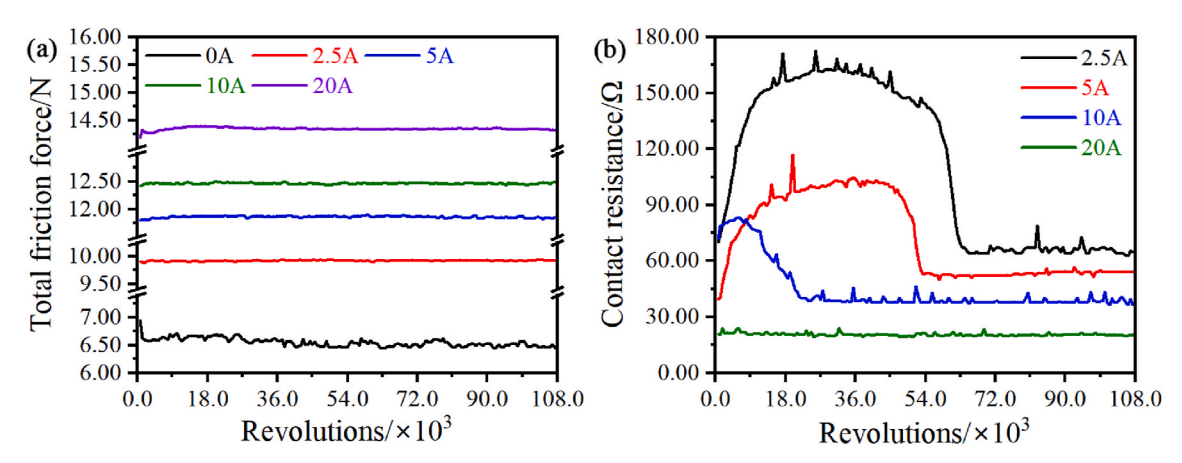


Fig. 3. Variation in (a) total friction force and (b) contact resistance at different currents.

value. Subsequently, the contact resistance remained stable, and it stabilized at 67.13, 56.27, 40.13, and 20.57 m $\Omega$  when the current increased from 2.5 to 20 A. In addition, the period of the first stage was

significantly shortened from 90 to 43 min as the electric current increased. The running-in process of contact resistance disappeared at  $20~\rm{A}.$ 

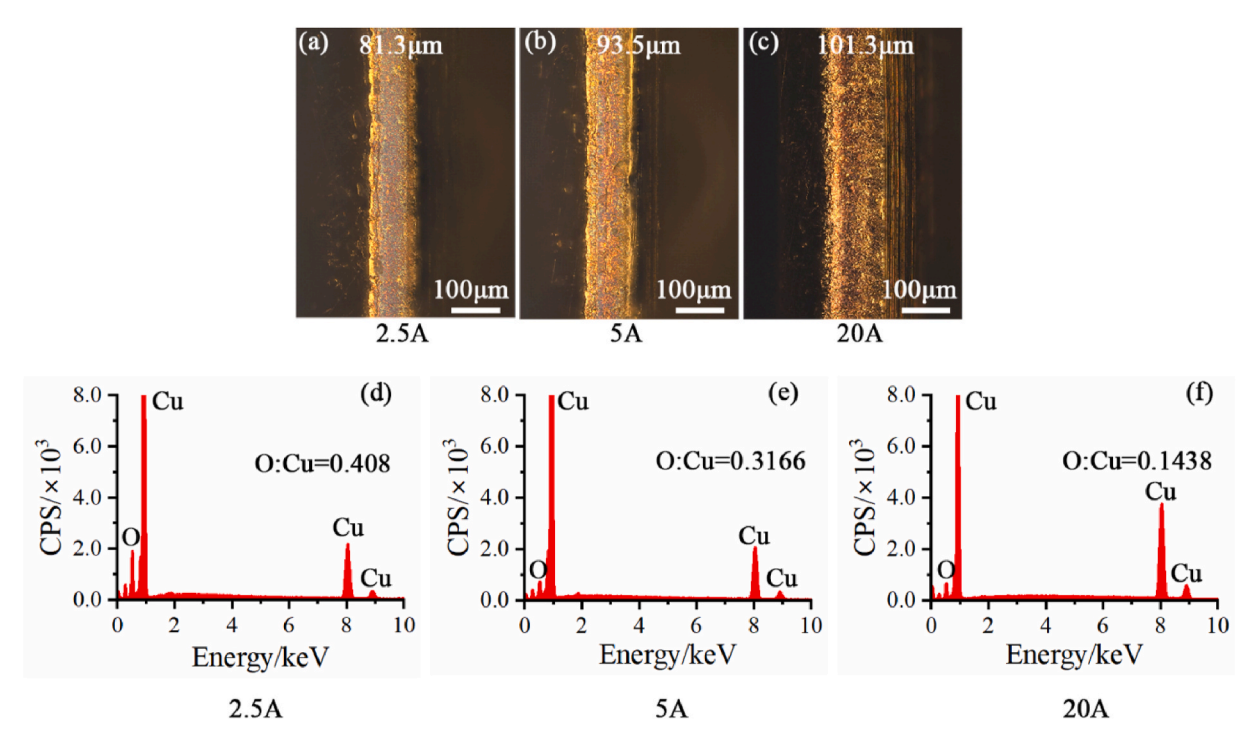


Fig. 4. Wear widths and corresponding EDS images at different electric currents after rolling to 27600 revolutions.

The observed contact resistance trends were owing to the metal wear that occurred between the contact pairs. In order to understand the wear characteristics of the roll-ring, the wear loss of roll-ring in different periods were measured. To explain the running-in process of the contact resistance, we detected the worn surface after 27600 rolling revolutions, and the results are shown in Fig. 4. We observed that belt-like wear scars formed on the contact area. Because the sharp contact surface was at an initial right angle, the contact pressure was sufficiently high to produce strong rheology at the early stage. As shown in Fig. 4a and b, the abrasion marks appeared smooth, and the products with black luster were observed at 2.5 and 5 A. On the surface rolled at 20 A, the abrasion marks were wider, and the metallic and black lusters were mixed (Fig. 4c). The EDS results in Fig. 4d–f indicate that the black product was CuO. The O:Cu atomic ratio decreased from 0.408 to 0.1438 as the current increased. During the running-in process, plastic deformation and oxidation occurred, and friction products were primarily maintained on the contact surface. The accumulation of oxide resulted in higher and unstable contact resistance in the running-in stage [11,12]. Therefore, the oxidation wear was the main mechanism in the running-in stage, particular for the lower current tests. Additionally, note that the oxidation degree of the surface at a higher current was lower, which indicated that the current promoted material wear. This was consistent with the sliding current-carrying wear phenomenon [5, 13,14].

The wear loss after rolling for different revolutions is showed in Fig. 5. Within the initial about 40000 revolutions, the wear loss is very low and the growth is slow. At higher revolutions, the wear amount increases significantly. The results show that the friction products accumulated on the contact surface at the early rolling stage, resulting in higher surface oxidation (Fig. 4) and higher contact resistance (Fig. 3). As the rolling continued, the oxide product was worn out, forming wear debris and leaving the underlying fresh metal. The contact between fresh metals can improve conductivity. Thus, an apparent decrease in contact resistance was observed in the second stage. Finally, wear marks with metallic lusters were formed. The higher electric current resulted in a wider wear area, and the average wear widths were 361.23, 379.04, 381.66, 391.74, and 403.34  $\mu m$  as the electric current increased from 0 to 20 A (Fig. 6). The widening of the wear marks provided a larger conductive area that was conducive to reducing the contact resistance.

The wear loss of the roll ring after the rolling test is shown in Fig. 7, which further demonstrates that a high current could result in severe damage to the roll ring. However, some differences were observed in the wear increments. As the current increased from 0 to 5 A, the average growth rate was 0.387. When the current exceeded 5 A, the wear increased significantly, and the average growth rate was approximately

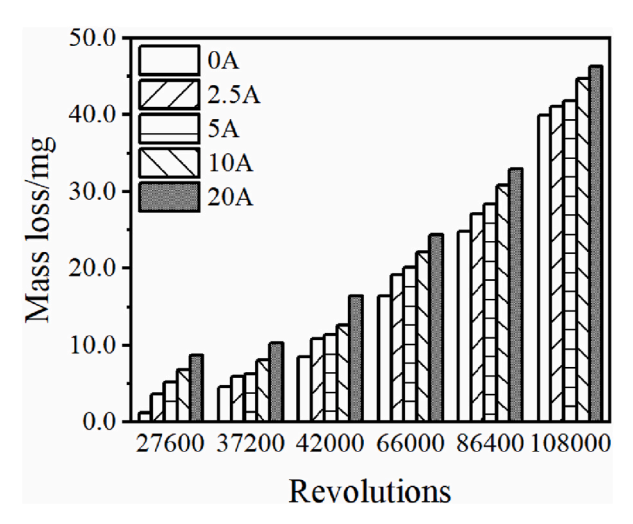


Fig. 5. The wear loss after rolling for different revolutions.

0.572. For the self-matching pairs, we assumed that the raceways suffered the same amount of mass loss as the roll rings. The wear volume of the raceways was equivalent to that of the boxes. The wear length was the circumference around the axis line at the contact position. Based on the wear width, wear length, and density of copper–beryllium alloy (7.633 g/cm³), the average wear thickness was 12.36, 12.54, 12.56, 12.86, and 13.03  $\mu m$ , as the electric current increased from 0 to 20 A. Wear thickness accounted for a very small proportion of the overall raceway.

## 3.2. Damage mechanism of the contact area

#### 3.2.1. Temperature increase

Friction heat is a key factor that affects metal dry wear. In the current-carrying friction process, the temperature increase in the contact pairs was the result of the coupling of heat sources from friction heat and Joule heat [15,16]. An infrared thermometer was used to measure the average temperature of the inner raceway. Fig. 8 shows the temperature as a function of the number of revolutions under different electric currents. The temperature curve under each test exhibited a gradually increasing and finally stable trend. The maximum temperature reached 34.8 °C at 20 A with a temperature increase of 14.8 °C, whereas the surface temperature at 0 A was 23.2 °C with a temperature increase of approximately 3.2 °C. A higher temperature can promote the mutual diffusion of metal atoms at the contact interface, resulting in a higher friction coefficient [17]. For a better understanding of the heat sources on the contact surface, the friction power and Joule heat power were calculated, as shown in Table 2.

The friction power  $P_{\text{tri}}$  was estimated using Equation (1):

$$P_{\rm tri} = FV, \tag{1}$$

where *F* is the friction force, and *V* is the linear velocity of the contact point between the roll ring and the inner raceway.

The Joule heat power  $P_{DC}$  was estimated using Equation (2):

$$P_{\rm DC} = I^2 R,\tag{2}$$

where I is the electric current, and R is the contact resistance.

The friction coefficient of the roll ring differs from that of conventional rolling. There were four contact areas between the roll ring and raceways, and the geometric change caused by wear can induce a decrease in the elastic preload. The average normal force and friction coefficient at a single contact point must be corrected; the results are shown in Fig. 9. After rolling for 108000 cycles, the single-point normal force decreased from 10.74 to 10.34 N with an increase in current. According to the total friction force obtained from the test, the friction coefficients of the single points were 0.15, 0.23, 0.28, 0.29, and 0.34. Therefore, the current-carrying friction coefficient was higher than the mechanical friction coefficient (0 A) and increased with the current.

# 3.2.2. Wear mechanism of the contact area

The tribo-informatics proposed by Zhang provides a new perspective for understanding the relationship between tribology performance and contact states. We are convinced that the wear profile is a direct feedback of the rolling current-carrying contact [18,19]. The morphologies of the worn roll-ring surfaces were observed using a 3D surface profiler (Fig. 10). At 0 and 2.5 A, a few gentle rough peaks were observed on the surface, and the corresponding surface roughness values were 0.725 and 0.845  $\,\mu m$ , respectively. When the current reached 5 A, corrugated morphology was detected, and the surface roughness increased to 1.143  $\,\mu m$ . Strong fluctuations occurred on the contact surface when the current increased to 10 and 20 A. A scaly morphology and sharp asperities occupied most of the wear area.

To obtain a better understanding of the current-carrying wear mechanism caused by the electric current, we obtained SEM images of the worn surfaces under different conditions. Fig. 11a shows the original

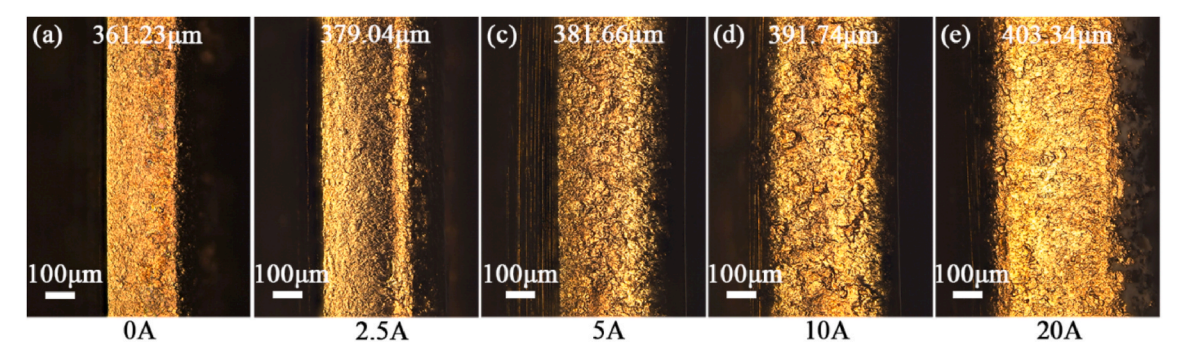


Fig. 6. Wear widths after rolling tests at different electric currents.

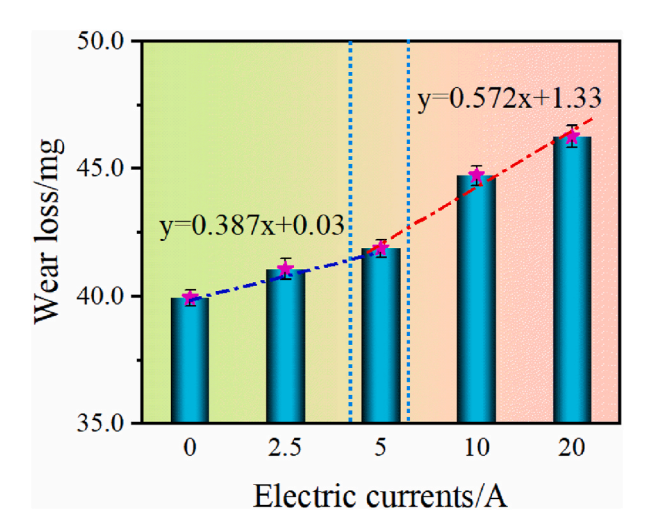


Fig. 7. Wear loss of the roll ring at the different currents.

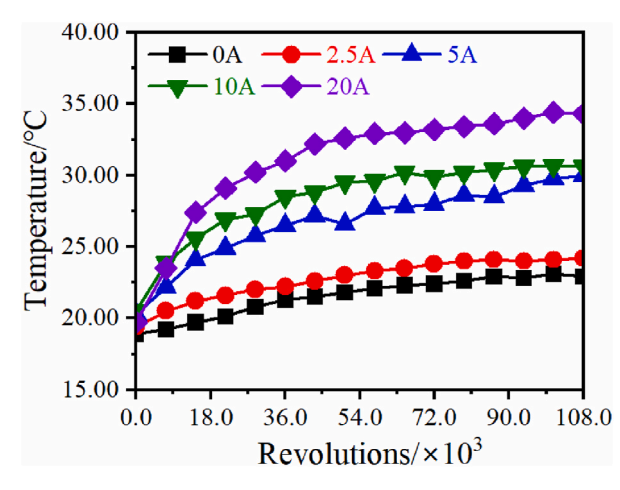


Fig. 8. Temperature at the contact surface on the inner raceway.

**Table 2** Friction and Joule heat power.

	0 A	2.5 A	5 A	10 A	20 A
Joule-thermal Power $P_{DC}$ (W)	0	0.42	1.41	4.01	8.23
Friction Power $P_{tri}$ (W)	12.17	17.54	21.17	22.29	25.61

surface of the roll ring before testing, which was smooth and flat. In the purely mechanical test shown in Fig. 11b, a large amount of intact surface remained, although a slight surface plastic deformation was

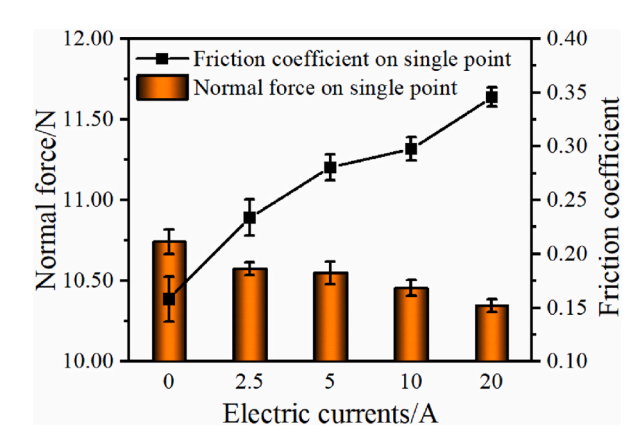


Fig. 9. Normal force and friction coefficient on a single contact point.

produced. As the current increased to 2.5 and 5 A, the contact surface suffered from noticeable plastic deformation accompanied by minor adhesion wear. At 10 A and 20 A, severe fatigue spalling caused a large amount of the flaky metal to fall off from the contact surface. The high friction coefficient induced by the large current caused the contact surface to bear high shear stress, which was prone to fatigue and spalling. Note that the fatigue level increased significantly from 5 to 10 A. These results were consistent with the wear losses mentioned above. Since the friction pairs were the same material of Copper-Beryllium C17200, adhesive wear should be unavoidable [20]. In particular, current-induced Joule heating can promote the adhesion of metals to contact surfaces [21]. The wear damage is the result of the joint action of fatigue wear, oxidation wear and adhesive wear. However, it is difficult to distinguish the adhesive transfer of the material on the SEM images because severe fatigue spalling, scaly delamination, and several surface cracks occupied the entire wear surface.

Fig. 12 shows the EDS results of oxygen and copper composition on the worn surfaces at different currents. The O:Cu ratio on the original surface was 0.062, and it decreased from 0.3275 to 0.1368 as the electric current increased on the wear surface. The oxidation degree of the current-carrying surface was higher than that of the original surface because of the tribo-oxidation and anodic oxidation of metal materials during rolling [21]. With the increase in current, the amount of products of anodic oxidation increased. However, the wear was more severe under a high current, and the removal of oxidation products was easier. The EDS results showed that the oxidation degree of the wear surface at a high current was relatively low, which was related to the wear removal of oxidation products. The generated nascent metal on the wear surface was beneficial to the conductivity. As a result, the contact resistance decreased at high currents (Fig. 3b).

Through previous performance test results and damage analysis, we observed that there was a contradiction between the friction and wear properties and electrical conductivity. The improvement in conductivity

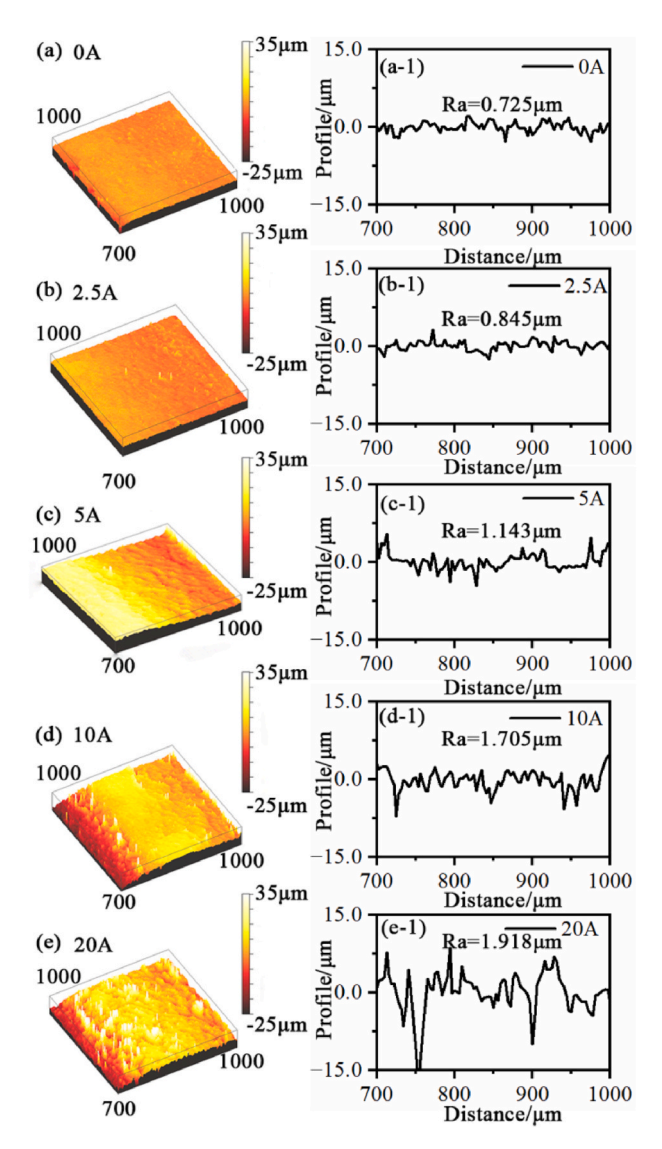


Fig. 10. Surface profile and roughness at different electric currents.

requires the sacrifice of the friction and wear properties. The synchronous improvement of conductivity and tribological properties will be a critical problem in the design of high-power rolling rings in the future.

## 3.2.3. Sub-surface damage mechanism

To discuss the material damage induced by the friction coefficient, we analyzed the microstructure below the worn surface in the longitudinal section using OM. As shown in Fig. 13a, equiaxed structures were observed in the original subsurface. The friction coefficient was 0.17 at 0 A, and no change occurred in grain size and shape (Fig. 13b). When the friction coefficient reached 0.24 (2.5 A), no grain deformation appeared on the subsurface, except for slight undulation near the contact area (Fig. 13c). When the friction coefficient increased to 0.28 (5 A), the grains below the contact surface were refined and deformed along the rolling direction, and the orientation of the grain boundaries tended to be parallel to the contact surface (Fig. 13d). After the current increased to 10 and 20 A, the friction coefficient increased to 0.31 and 0.35, respectively. The grains near the contact surface were severely damaged, and the grain shape and boundaries were no longer distinguishable. Fierce undulation caused by material peeling was observed on the subsurface (Fig. 13e and f).

The results in Fig. 13 show that the surface layer of the contact area may have been recrystallized under 10 and 20 A conditions. However, at 20 A, the temperature of the roll ring was 307.9 K, which was far from the recrystallization temperature [22]. Zhu et al. [23] reported that a high-density current can induce a sharp decrease in the deformation resistance of a metal and increase its plasticity [24-27]. The current density in this study was simulated using the software COMSOL Multiphysics. As shown in Fig. 14, when the applied current increased from 2.5 to 20 A, the current density increased from  $1.71 \times 10^2$  to  $4.19 \times 10^2$ A/mm<sup>2</sup>. When high-density current flowed through the metal material, drift electrons formed inside the material. With the aid of drift electrons, the movement of vacancies and dislocations improved, which accelerated dislocation annihilation, resulting in a reduction in the flow stress and plastic strain [28,29]. We speculated that when the current density exceeded 409 A/mm<sup>2</sup>, an electroplastic effect occurred beneath the contact surface.

To test this hypothesis, we used EBSD maps to highlight the regions where plastic deformation occurred. The grain map in Fig. 15a indicates that no grain deformation occurred in the original sample. The grains inclined along the rolling direction, and the number increased after the rolling test at 5 A (Fig. 15b). When the current reached 20 A (Fig. 15c), a

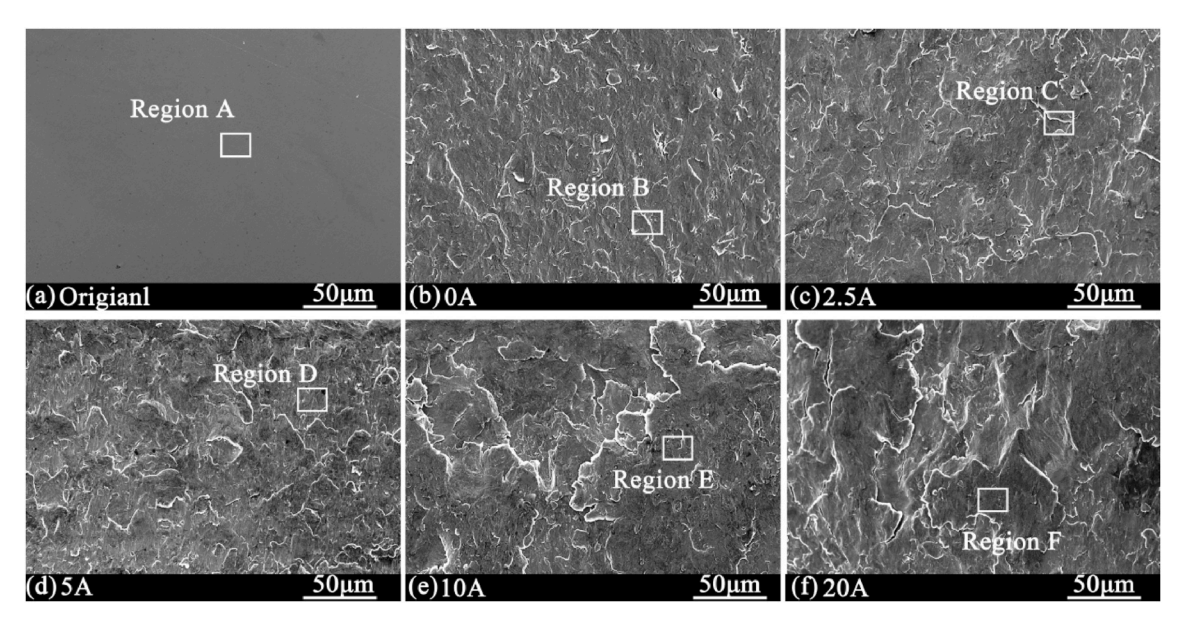


Fig. 11. SEM micrographs of the worn surfaces after rolling tests: (a) Original; (b) 0 A; (c) 2.5 A; (d) 5 A; (e) 10 A; (f) 20 A.

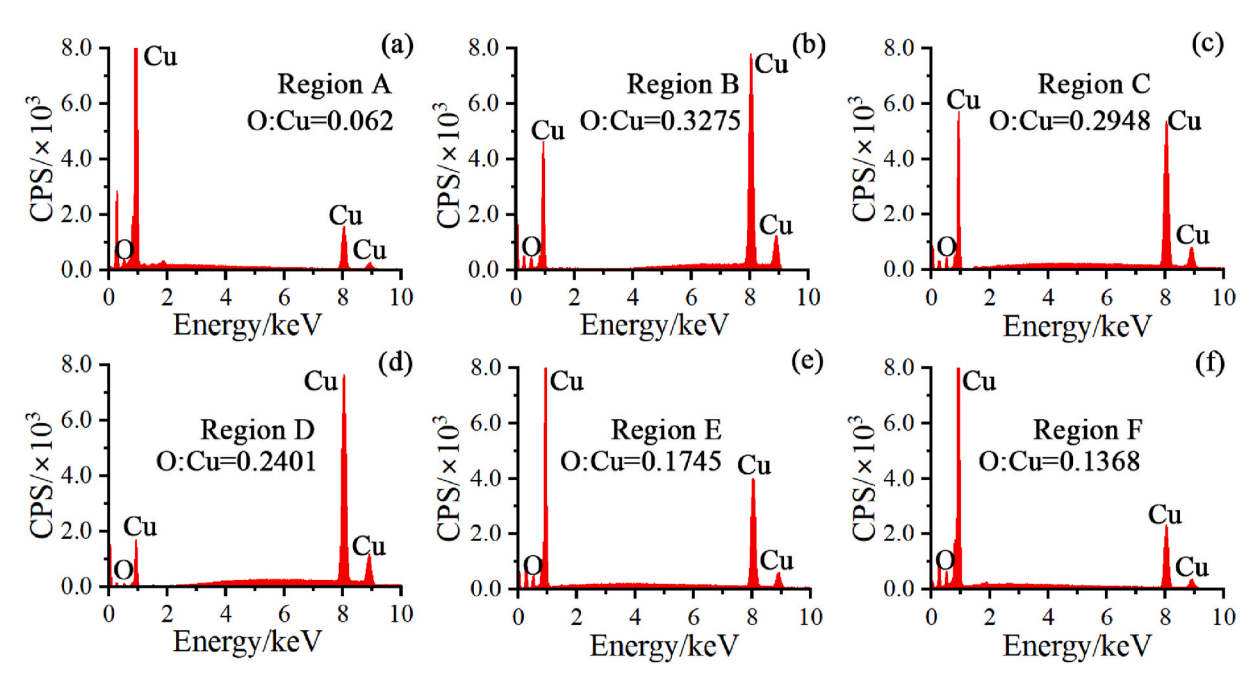


Fig. 12. EDS results of the selected area from Fig. 9: (a) Region A; (b) Region B; (c) Region C; (d) Region D; (e) Region E; (f) Region F.

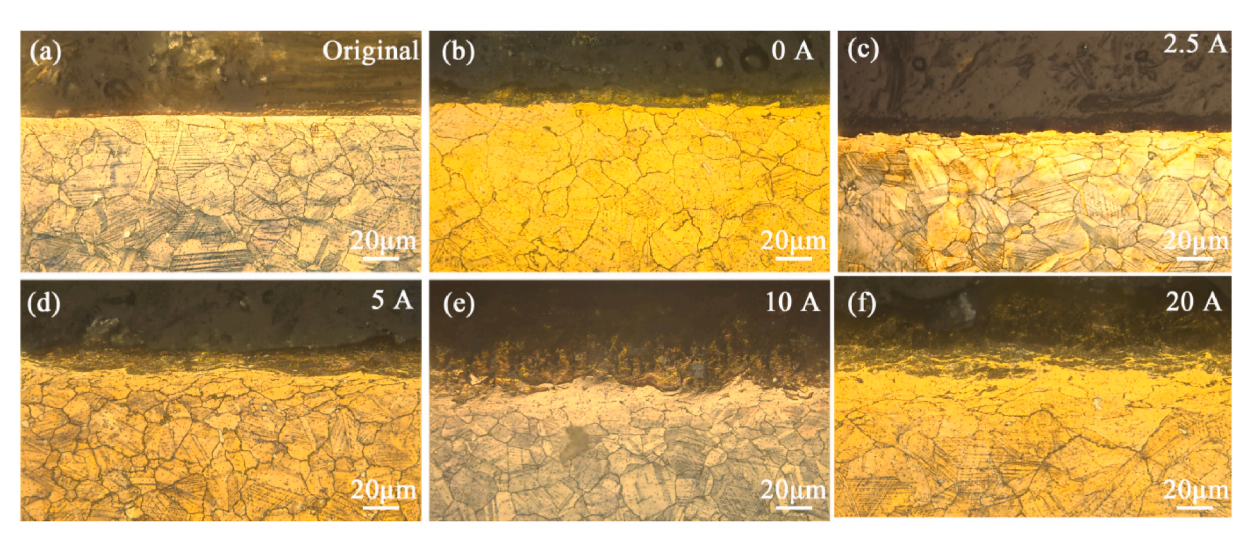


Fig. 13. Optical microscopy (OM) images of the roll-ring longitudinal section after rolling tests. (a) Original sample; (b) 0 A; (c) 2.5 A; (d) 5 A; (e) 10 A; (f) 20 A.

small number of vague grain boundaries existed near the contact surface. The stress concentration induced by grain deformation could be illustrated using the corresponding kernel average misorientation (KAM) maps. Compared with that under the original surface (Fig. 15d), the stress concentration under the contact surface after rolling at 5 A was more significant (Fig. 15e). This means that rolling produced congestion and proliferation of dislocations at the grain boundaries and in the grains. However, the stress concentration was significantly weakened after testing at 20 A (Fig. 15f). This indicated that the electroplastic effect of a high-density current can promote the movement and annihilation of the boundaries and dislocations. The EBSD results were consistent with the OM results.

Different microstructures and stress states of materials inevitably result in changes in their mechanical properties. The microhardness values in the depth direction beneath the worn surface under different currents are shown in Fig. 16. A hardness transformer layer was observed below the rolling surface. This hardening was caused by the grain refinement and stress concentration caused by rolling (Figs. 13 and

15). With an increase in the test depth, the hardness returned to the matrix value of 428 HV $_{200g}$ . The thickness of the hardness transformer layer generally did not exceed 250  $\mu$ m. The surface hardness changed significantly at different current. For example, the surface hardness at a depth of 15  $\mu$ m, under different currents, first increased and then decreased. The hardness reached a maximum value of 481.6 HV $_{200g}$ . The results in Fig. 14 show that hardening of surface played a dominant role in the range of 0–5 A. At this stage, a high friction coefficient induced by the current could result in sufficient dislocation multiplication, packing, grain refinement, and stress concentration (Figs. 13 and 15). When the current exceeded 10 A, the electroplastic effect of the current weakened the hardening effect and the surface hardness decreased. Therefore, the growth slope of the wear amount was higher at 10 and 20 A (Fig. 7).

By analyzing the metallography, grain size, stress, and hardness of the subsurface layer, the influence mechanism of the current on the wear was revealed, and hardening and softening of the rolling surface were distinguished at different current in detail. Note that there was a strong strain-rate sensitivity to hardness. Reference [30,31] reported a positive

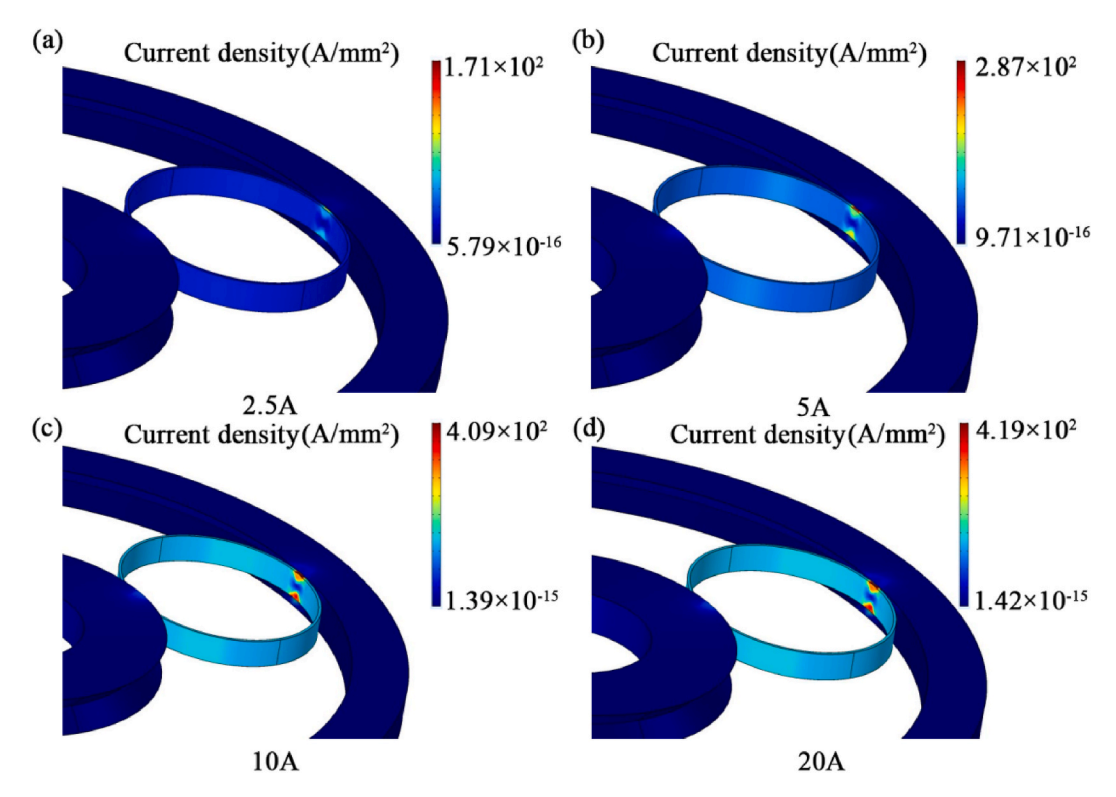


Fig. 14. Current density at different electric currents.

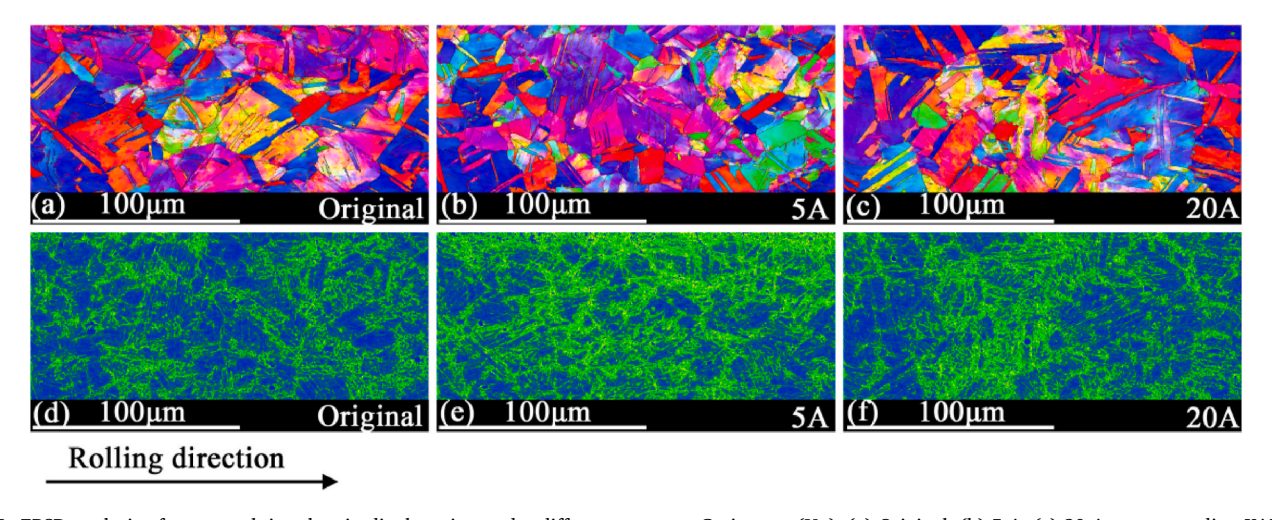
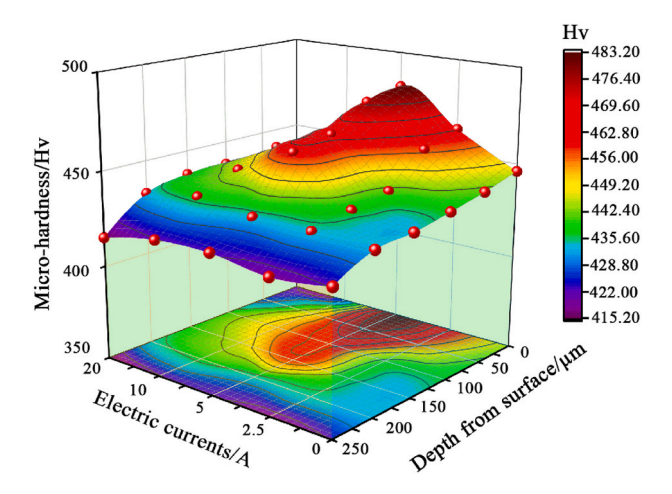


Fig. 15. EBSD analysis of wear track in a longitudinal section under different currents. Grain map (Up): (a) Original; (b) 5 A; (c) 20 A; corresponding KAM map (Down): (d) Original; (e) 5 A; (f) 20 A.

correlation between hardness and strain rate. Considering the size of contact pairs and the width of the wear scar (361.23–403.34  $\mu m$  in this study), the contact between the roll ring and raceways can be equivalent to a line contact. According to the contact mechanism [32], the maximum shear stress was estimated to be 62.8–59.6 MPa, and the contact length along the rolling direction was 157.2–166.3  $\mu m$ . At a speed of 600 r/min, the loading time was approximately 8.74  $\times$   $10^{-5}$ –9.29  $\times$   $10^{-5}$  s; thus, the strain rate during rolling was 3.59  $\times$   $10^{5}$ –2.69  $\times$   $10^{6}$  1/s. Because the strain rate during rolling was much higher than that during hardness, the real-time hardness during rolling may have been higher than the measured value.

In summary, the current-carrying tribological properties of the roll ring were tested at different electric currents. A contradiction between the friction and wear properties and the electrical conductivity was observed. The effects of current on the surface hardness and wear were discussed. Compared with the rigid disk–disk contact [11], no arc discharge occurred during rolling owing to the natural advantages of the adaptive flexible contact. The current density of the rolling electrical contact exceeded 400 A/mm², which was significantly higher than that of the traditional sliding electrical contact [3]. The results showed that a single roll ring could transmit a current of 20 A, and if multiple rings are connected in parallel in the raceways, the transmission capacity can be further improved. However, the conductive rotary joint in applications requires that the life of the roll ring should exceed 10<sup>7</sup> revolutions, and the maintenance-free function should be reached within the life cycle. Under the test conditions in this study, the wear amount after 10<sup>5</sup> revolutions exceeded 40 mg, and the wear surface exhibited severe fatigue peeling. In follow-up research, attention should be given to slowing



**Fig. 16.** Work hardening of wear area: Microhardness in the depth direction beneath the wear surface.

down wear, reducing fatigue, preventing oxidation, etc. The results presented here may provide a reference for the failure analysis and design of high-power and long-life rolling conductive rotary joints.

#### 4. Conclusions

The tribological and conductive behaviors of the roll rings under different electric currents were examined using a rolling tribometer. The conclusions are summarized as follows:

- 1. As the electric currents increased from 0 to 20 A, the total friction force in the steady-state period increased from 6.8 to 14.31 N, and the contact resistance decreased from 67.13 to 20.57 m $\Omega$ . The decrease in contact resistance was related to the increase in the wear area and removal of tribo-products from the contact surface.
- The current caused surface oxidation as well as a high friction coefficient and material peeling. As the current increased, the wear amount increased, and the degree of surface oxidation decreased.
- 3. The current has two effects on surface hardness: hardening and softening. The EBSD results and hardness tests showed that the surface hardness was dominated by hardening when the current density was lower than 409 A/mm², and the softening was more apparent at higher current densities. The surface hardness was highest at 5 A.

### **Author statement**

Material preparation, data collection and analysis were performed by Tianhua Chen, Chenfei Song, Zili Liu. The manuscript and figures were prepared by Tianhua Chen, Li Wang and Huanhuan Lu. The test scheme was designed by Xinbin Hou and Yongzhen Zhang. All authors read and approved the final manuscript.

# Declaration of competing interest

The authors declare that they have no known competing financial interests or personal relationships that could have appeared to influence the work reported in this paper.

# Data availability

The authors do not have permission to share data.

# Acknowledgement

This work was supported by the National Key Research and

Development Program of China (2020YFB2007900), the National Natural Science Foundation of China (52275185), the Natural Science Foundation of Henan Province (202300410123).

#### References

- C. Liu, X. Chen, Z. Qian, Research on the friction pair of the space high-power and long-life rolling ring, IOP Conf. Ser. Mater. Sci. Eng. 638 (2019), 012005.
- [2] B. Luo, C. Liu, X. Liu, L. Zhang, Effect of expanded graphite on the tribological behavior of tin-bronze fiber brushes sliding against brass, Tribol. Trans. 63 (2019) 1–8
- [3] G. Mei, W. Fu, G. Chen, W. Zhang, Effect of high-density current on the wear of carbon sliders against Cu–Ag wires, Wear (2020) 452–453, 203275.
- [4] T. Ding, G.X. Chen, Z.G. Xiong, L. Xie, C.X. Wu, The role of electric current on friction and wear behaviors of the carbon strip/copper contact wire, Appl. Mech. Mater. 80–81 (2011) 178–181.
- [5] W. Ren, P. Wang, J. Song, G. Zhai, Effects of current load on wear and fretting corrosion of gold-plated electrical contacts, Tribol. Int. 70 (2014) 75–82.
- [6] Y. Feng, M. Zhang, Y. Xu, Effect of the electric current on the friction and wear properties of the CNT-Ag-G composites, Carbon 43 (2005) 2685–2692.
- [7] V.V. Fadin, M.I. Aleutdinova, A.V. Kolubaev, Effect of high-density electric current on wear and average temperature of steel/steel triboelectric contact, J. Frict. Wear 39 (2018) 294–298.
- [8] T. Chen, C. Song, Y. Zhang, K. Niu, Z. Liu, L. Wang, C. Sun, M. Li, Y. Zhang, Current-carrying contact character and wear behavior of an elastic ring at different rolling speeds, Eng. Fail. Anal. 131 (2022), 105825.
- [9] C. Niu, J. Chen, F. Yang, Q. Liu, H. Lei, Y. Wu, Y. Wu, M. Rong, Investigation of the electrical rolling contact degradation based on fractal theory, Eng. Fail. Anal. 113 (2020), 104559.
- [10] Z. Wang, J. Li, Y. Zhang, C. Lv, T. Li, J.Q. Zhang, S.X. Hui, L.J. Peng, G.J. Huang, H. F. Xie, X.J. Mi, Comparison of the mechanical properties and microstructures of OB2.0 and C17200 alloys, Materials 15 (2022) 2570.
- [11] J. Li, C. Song, Y. Zhang, Y. Sun, T. Chen, L. Wang, Z. Liu, S. Wang, Y. Zhang, Effect of rotation speed on the tribological and conductive behaviors of rolling currentcarrying Cu pairs, Mater. Trans. 62 (2021) 453–460.
- [12] Z.L. Hu, Z.H. Chen, J.T. Xia, Study on surface film in the wear of electrographite brushes against copper commutators for variable current and humidity, Wear 264 (2008) 11–17.
- [13] H. Yang, B. Hu, Y. Liu, X. Cui, G. Jiang, Influence of reciprocating distance on the delamination wear of the carbon strip in pantograph-catenary system at high sliding-speed with strong electrical current, Eng. Fail. Anal. 104 (2019) 887–897.
- [14] D.G. Bansal, J.L. Streator, Behavior of copper-aluminum tribological pair under high current densities, IEEE Trans. Magn. 45 (2009) 244–249.
- 15] X. Zuo, M. Du, Y. Zhou, Influence of contact parameters on the coupling temperature of copper-brass electrical contacts, Eng. Fail. Anal. 136 (2022), 106205.
- [16] T. Ding, G.X. Chen, Z.G. Xiong, L. Xie, C.X. Wu, The influence of the temperature in severe wear of copper contact wire/carbon strip under electric current, Appl. Mech. Mater. 71–78 (2011) 3653–3656.
- [17] A. Gåård, N. Hallbäck, P. Krakhmalev, J. Bergström, Temperature effects on adhesive wear in dry sliding contacts, Wear 268 (2010) 968–975.
- [18] N. Yin, Z. Xing, K. He, Z. Zhang, Tribo-informatics approaches in tribology research: a review, Friction 11 (2022) 1–22.
- [19] Z. Zhang, N. Yin, S. Chen, C. Liu, Tribo-informatics: concept, architecture, and case study, Friction 9 (2020) 642–655.
- [20] V. Chaudhry, S.V. Kailas, Fretting studies on self-mated stainless steel and chromium carbide coated surfaces under controlled environment conditions, Wear 301 (2013) 524–539.
- [21] Y.P. Chang, J.P. Yur, H.M. Chou, H.M. Chu, Tribo-electrification mechanisms for self-mated carbon steels in dry severe wear process, Wear 260 (2006) 1209–1216.
- [22] Z. Zhao, J. Liu, S. Lu, Y. Xiao, M. Yuan, Deformation mechanisms in highly elastic softened-state Cu–Be alloy at elevated temperatures, Phys. Met. Metallogr. 119 (2018) 69–75.
- [23] R.F. Zhu, G.Y. Tang, S.Q. Shi, M.W. Fu, Effect of electroplastic rolling on the ductility and superelasticity of TiNi shape memory alloy, Mater. Des. 44 (2013) 606–611.
- [24] M. Breda, I. Calliari, S. Bruschi, M. Forzan, A. Ghiotti, F. Michieletto, M. Spezzapria, C. Gennari, Influence of stacking fault energy in electrically assisted uniaxial tension of FCC metals, Mater. Sci. Technol. 33 (2016) 317–325.
- [25] T. Jiang, L. Peng, P. Yi, X. Lai, Investigation of deformation behavior of SS304 and pure copper subjected to electrically assisted forming process, J. Manuf. Sci. Eng. 139 (2017) 1–12.
- [26] R.F. Zhu, J.N. Liu, G.Y. Tang, S.Q. Shi, M.W. Fu, Properties, microstructure and texture evolution of cold rolled Cu strips under electropulsing treatment, J. Alloys Compd. 544 (2012) 203–208.
- [27] D. Li, E. Yu, Z. Liu, Microscopic mechanism and numerical calculation of electroplastic effect on metal's flow stress, Mater. Sci. Eng., A 580 (2013) 410–413.
- [28] S. Xiang, X. Zhang, Dislocation structure evolution under electroplastic effect, Mater. Sci. Eng., A 761 (2019), 138026.
- [29] X. Zhang, H. Li, M. Zhan, Mechanism for the macro and micro behaviors of the Nibased superalloy during electrically-assisted tension: local Joule heating effect, J. Alloys Compd. 742 (2018) 480–489.

[30] G.H. Majzoobi, J. Mohammadi, M.K. Pipelzadeh, S. Lahmi, S.J. Hardy, A constitutive model for hardness considering the effects of strain, strain rate and temperature, J. Strain Anal. Eng. Des. 50 (2015) 284–298.

- [31] G.S. Xiao, G.Z. Yuan, C.N. Jia, X.X. Yang, Z.G. Li, X.F. Shu, Strain rate sensitivity of Sn-3.0Ag-0.5Cu solder investigated by nanoindentation, Mater. Sci. Eng., A 613 (2014) 336–339.
- [32] K.L. Johnson, Contact Mechanics, Cambridge University Press, 1987.